Thermal Optimization of Heat Sink for Inverter Applications

F. Onoroh[1], M. Ogbonnaya[1], J. L. Chukuneke[2], C. B. Echeta[2]

[1]Department of Mechanical Engineering, University of Lagos, Akoka, Yaba, Lagos state, Nigeria
[2]Department of Mechanical Engineering, Nnamdi Azikiwe University, Awka, Anambra state, Nigeria
E-mail: onofrankus@yahoo.com

Abstract. Power inverters enable efficient conversion of DC voltage and current to AC voltage and current and are intermediate device in renewable energy technology application especially solar, wind and thermoelectric energy. The key technologies behind power inverters switching operation are the semiconductor devices such as the IRF 3205 MOSFET chip. During operation the switches dissipate heat and if the dissipated heat is not properly managed, thermally induced failure may occur. The research work involves generation of a heat sink model and its optimization for a 24VDC/2.5K.V.A inverter. The thermal resistance, fval, of the optimized heat sink was found to be equal to 0.0345 ^{o}C/W which is less than the thermal resistance of the heat sink to ambient of the IRF 3205 MOSFET switch of 0.5063 ^{o}C/W. The thermal management of the power inverter package yields experimental and modeled package temperatures of 34.7^{o}C and 36.5^{o}C respectively. The optimized heat sink using the model created leads to reduction in size, weight and reliable operation of the power inverter.
Keywords. Power inverter; Renewable energy; Reliability; Heat Sink; Thermal resistance; MOSFET chip; Failure.

1.Introduction

Power inverter involves the conversion of electric power from direct voltage and current levels to alternating voltage and current levels. Power electronics is now a major part of power engineering; at least 25% of all power generated passes through some form of electronic system before being utilized [1].

In the inverter, DC power from the battery bank is inverted to AC power via a set of solid state switches – MOSFETs or IGBTs that essentially flip the DC power back and forth creating AC power [2][3]. In the course of the inversion, electrical power is dissipated as thermal energy, and reliability of the power inverter can be compromised if accurate thermal management is not put in place [4].

Problems associated with the thermal dissipation and heat transfer through power inverters is one of the most urgent issues that requires significant attention in order to produce efficient and reliable electrical energy conversion systems [5].

In a typical MOSFET base power inverter, power is dissipated as heat. To avoid unacceptable temperature rises to prevent thermal problems, improvements in cooling methods are obligatory [6]. The heat generated as a result of these losses must be conducted away from the power devices and into the environment using a heat sink. If an appropriate thermal system is not used, elevated temperatures can adversely affect electronic device operation; power handling capability, reliability and even risk of electrical fire outbreak. It has been showed that more than 55% of the electronic failures are caused by heat [7].

2.Thermal Dissipation in a Power Inverter

Heat energy can be transferred from one place to another by conduction, convection and radiation. These phenomena may take place in a given system singly or simultaneously. However, the majority of heat generated by the IRF 3205 MOSFET switches in a power inverter is transported via conduction to the bottom of the switches. Other mechanisms are seldom sufficient to cause any noticeable change [8][9].
As a result of heat dissipation during the switching operation of the IRF3205 MOSFET chips, thermal management system must be optimized to attain the highest performance of the inverter. However in other to optimize the overall heat sink, thermal performance is usually maximized and the weight satisfying constraints are minimized.

The main components that make the power module stack are the die, the solder and the base-plate. The IRF 3205 MOSFET chip is fastened to the heat sink with the aid of screw. In this configuration, the heat generated in the die is conducted down through the stack to the base-plate which is then cooled by the heat sink via air circulation. Extended surface is used specially to enhance the heat transfer rate between a solid and an adjoining fluid. The heat sink is a high thermal mass attached to the base-plate enabling it to help reduce the die temperature during operation [10][11].
Variations to the heat sink geometry and material allow the heat sink to be optimized. An understanding of the way in which the material of the heat sink affects its performance is required to inform about cost and performance as given by the coefficient of heat penetration, (CHP).

Heat sink with a higher CHP reduces the die temperature more as the material have a low thermal resistance and high thermal capacitance. The CHP describes how much thermal capacity is available within the early period of the heat flow and is obtained directly from the material properties as:

$$\mathrm{CHP} = \sqrt{k\rho C_p} \tag{1}$$

Where k is the thermal conductivity of the material, W/mK, ρ is the density of the material, kg/m^3, Cp is specific heat capacity of the material, J/kgK.

3.Generation of Heat Sink Model

Figure 1 shows the geometry of an extruded heat sink and the associated thermal resistance network. Using the definitions, of the heat sink geometry as shown in figure 1, the fin spacing ratio k_f is defined as [12]:

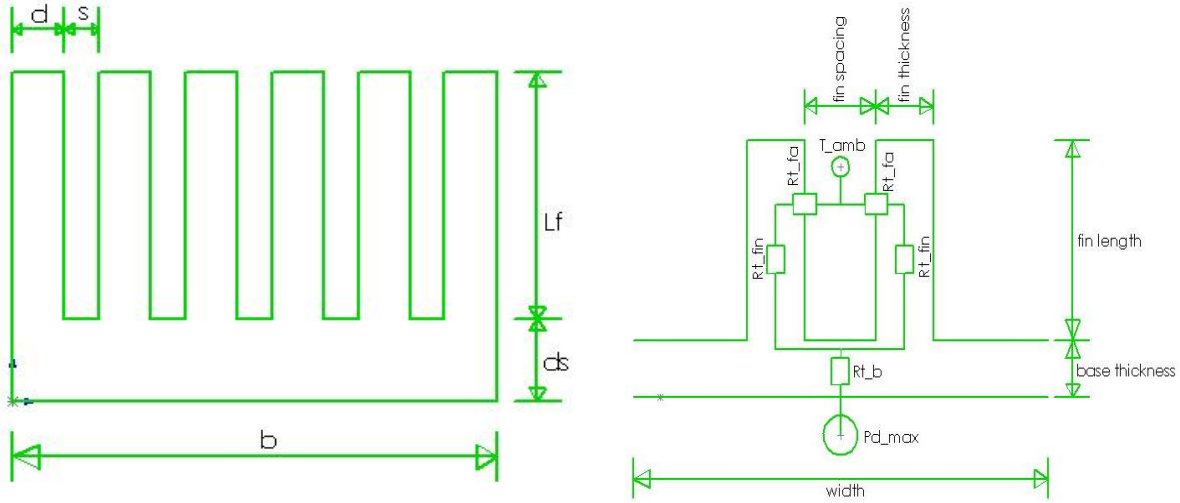

Fig. 1 Geometry of an Extruded Heat Sink

$$k_f = \frac{s(n-1)}{b} \tag{2}$$

Where s is the air passage width, m, b is the distance between the first and last fins, m, n is the number of fins. With values between zero and one, the fin spacing ratio characterizes the cross section of the heat sink available for air flow. The hydraulic diameter, d_h, is a commonly used term when handling flow in noncircular tubes and channels. It can be expressed as a function of the heat sink geometry as:

$$d_h = \frac{4A}{p} \tag{3}$$

Where A is the area of duct section perpendicular to the flow, it can be expressed as:

$$A = (n-1)s \cdot L_f \tag{4}$$

P is the wetted perimeter of the duct, it can be expressed as:

$$P = 2(n-1)(s + L_f) \tag{5}$$

In the light of equation (4) and equation (5), the hydraulic diameter of the fluid channel is obtained as [13]:

$$d_h = \frac{2sL_f}{s+L_f} \tag{6}$$

Where L_f is the fin length, m. For a given fin geometry, the total air flow through all channels creates a pressure drop along the heat sink length, L, into the paper which is given for laminar flow as [14]:

$$\Delta P_L = 1.5 \frac{32\rho\upsilon L}{n(sL_f)d_h^2}\dot{V} \tag{7}$$

Where ρ is the density of air, υ is the kinematic viscosity of air, m^2/s, $\dot{V}$ is volume flow rate of air m^3/s. The 1.5 correction factor takes into account the non quadratic channel shape characterized by $s \ll L_f$. In the case of turbulent flow, the pressure drop is given as [14]:

$$\Delta P_T = \frac{L\frac{s+L_f}{2sL_f}\rho\frac{1}{2}\left(\frac{\dot{V}^2}{n(sL_f)}\right)^2}{\left(0.79\ln\left(\frac{2\dot{V}}{n(s+L_f)\upsilon}\right)-1.64\right)^2} \tag{8}$$

For laminar flow the Nusselt number, Nu, can be obtained as [14]:

$$Nu_L = \frac{3.657\left[\tanh\left(2.264X^{1/3}+1.7X^{2/3}\right)\right]^{-1}+\frac{0.0499}{X}\tanh X}{\tanh\left(2.432Pr^{1/6}X^{1/6}\right)} \tag{9}$$

With

$$X = \frac{L}{d_h RePr} \tag{10}$$

$$Pr = \frac{C_p\mu}{k} \tag{11}$$

μ is the dynamic viscosity, kg/ms.

While the Nusselt number, Nu, for Turbulent flow is [14]:

$$\mathrm{Nu_T} = \frac{\left[8(0.79\ln \mathrm{Re}-1.64)^2\right]^{-1}(\mathrm{Re}-1000)\mathrm{Pr}}{1+12.7\sqrt{\left[8(0.79\ln \mathrm{Re}-1.64)^2\right]^{-1}}\left(\mathrm{Pr}^{2/3}-1\right)\left(1+\left(\frac{\mathrm{d_h}}{\mathrm{L}}\right)^{2/3}\right)} \tag{12}$$

Therefore, the heat transfer coefficient is obtained from the Nusselt number as [15][16]:

$$\mathrm{h_c} = \frac{\mathrm{Nuk}}{\mathrm{d_h}} \tag{13}$$

The Reynolds number, Re, of the fluid can be expressed as a function of the heat sink geometry is as follows:

$$Re = \frac{\rho u D_h}{\mu} \tag{14}$$

Using the concept of kinematic viscosity, the Reynolds number can be expressed as:

$$Re = \frac{u D_h}{\upsilon} \tag{15}$$

From the definition of the hydraulic diameter of equation (3), equation (15) can be expressed as:

$$Re = \frac{4\dot{V}}{\upsilon \mathrm{P}} \tag{16}$$

Substituting equation (5) into equation (16), the Reynolds number as a function of the heat sink profile of figure 1 is then obtained as:

$$Re = \frac{2\dot{V}}{\upsilon(\mathrm{n}-1)(\mathrm{s}+\mathrm{L_f})} \tag{17}$$

If the Reynold's number, Re, is less than 2300, the flow is laminar, otherwise it is turbulent. All properties of air are evaluated at the mean film temperature, T_f, as [17][18]:

$$\mathrm{T_f} = \frac{\mathrm{T_b}+\mathrm{T_\infty}}{2} \tag{18}$$

The significant thermal performance index for efficient heat dissipation is the thermal resistance, $R_{t,hs}$, of the heat sink, which comprises the thermal resistance of the heat sink base, $R_{t,b}$, thermal resistance between fin surface and the air channel, $R_{t,fa}$, the thermal resistance of the fin, $R_{t,fin}$, as shown in figure 1, for an air channel.

The resultant thermal resistance of the heat sink by application of series and parallel combination of resistance yields the thermal resistance of the heat sink as:

$$\mathrm{R_{t,hs}} = \frac{1}{\mathrm{n}}\left\{\frac{\left(\frac{1}{\mathrm{h_C A_{fa}}}+\frac{\frac{1}{2}\mathrm{L_f}}{\frac{1}{2}\delta \mathrm{Lk_{al}}}\right)\left(\frac{1}{\mathrm{h_C A_{fa}}}+\frac{\frac{1}{2}\mathrm{L_f}}{\frac{1}{2}\delta \mathrm{Lk_{al}}}\right)}{2\left[\left(\frac{1}{\mathrm{h_C A_{fa}}}\right)+\left(\frac{\frac{1}{2}\mathrm{L_f}}{\frac{1}{2}\delta \mathrm{Lk_{al}}}\right)\right]}\right\}+\left(\frac{\mathrm{d}}{\frac{1}{\mathrm{n}}\mathrm{A_b k_{al}}}\right) \tag{19}$$

Under operating conditions, the thermal resistance between the IRF 3205 MOSFET chip/heat sink assembly, is defined as:

$$R_{t,sa} = \frac{T_j - T_\infty}{P_{dmax}} - \left(R_{t,jc} + R_{t,cs}\right) \quad (20)$$

For effective heat dissipation, the necessary condition to be satisfied is:

$$R_{t,hs} \leq R_{t,sa} \quad (21)$$

The convective heat transfer is obtained from the relation:

$$\dot{Q} = \frac{T_j - T_c}{R_{t,hs}} \quad (22)$$

Where d is the heat sink base thickness, m, A_{fa} is the effective convective surface area of air channel, m^2, k_{hs} is the thermal conductivity of heat sink material, W/mK, L is the heat sink length, m, L_f is the fin height, m, δ is the fin thickness, m, T_j is the junction temperature, ^oC, T_∞ is the ambient temperature, ^oC, T_c is the case temperature, ^oC, P_{dmax} is the maximum dissipated power, W, $R_{t,jc}$ is the junction to case thermal resistance, $^oC/W$, $R_{t,cs}$ is the case to heat sink thermal resistance, $^oC/W$.

4.Results and Discussion

The critical thermal performance parameters of the generated heat sink model are fin spacing, fin thickness, length of fin, length of heat sink and number of fins. The heat sink model is simulated in MATLAB, to show the influence of each parameter on the heat sink performance. The calculation procedure is as shown in the flow diagram of figure 2.

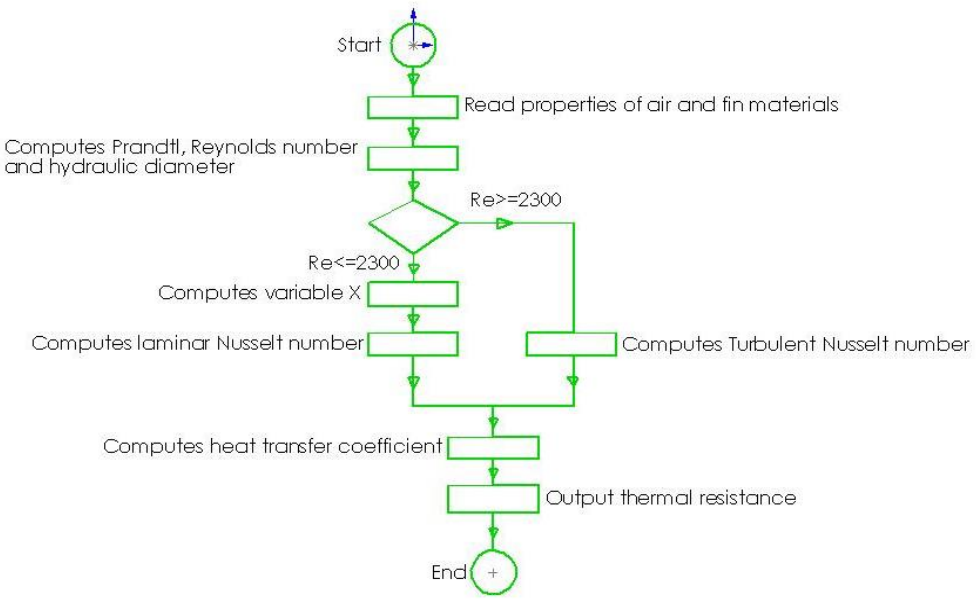

Fig. 2 Heat Sink Model Simulation Flow Diagram

4.1 Variation of Thermal Resistance with Fin Spacing and Number of Fins

Figure 3 shows the 3-D and 2-D plot of thermal resistance with fin spacing and number of fins. From the plots increasing the fin spacing and number of fins, results in a decrease in the thermal resistance of the heat sink, and thus an increase in heat dissipation capability of the heat sink. This is as expected as increasing fin spacing leads to an increase in effective heat transfer area for heat transfer to take place.

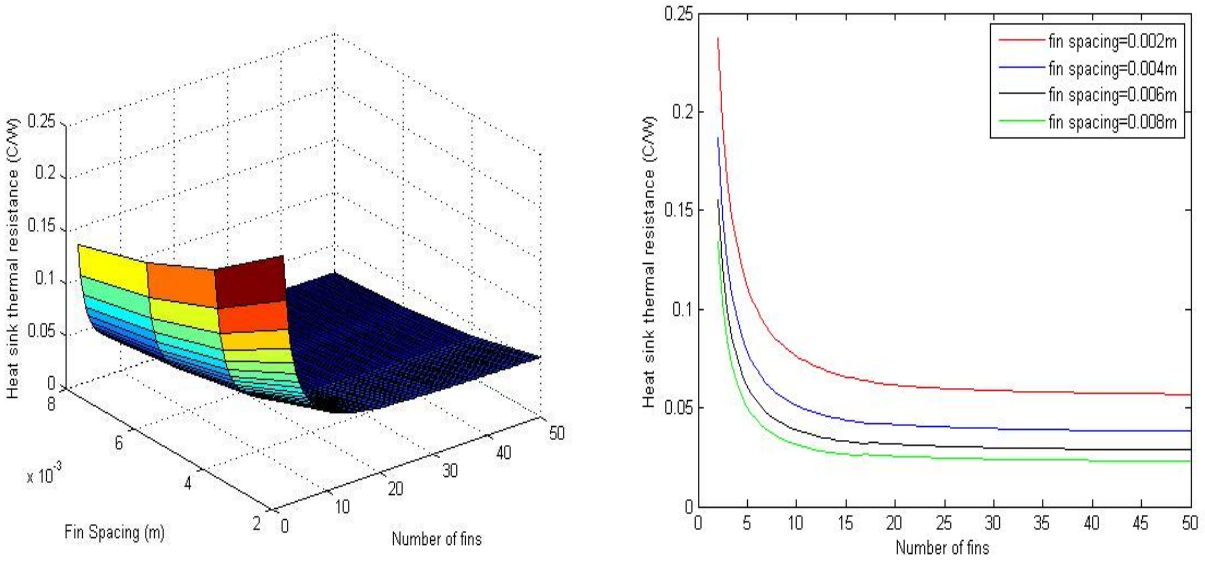

Fig. 3 Thermal Resistance Curves at various Fins spacing and number of Fins

However, for a constant heat sink width, increasing the number of fins means a corresponding decrease in the fin spacing/or thickness of the fin. Thus, the fin spacing ratio characterizes the cross section of the heat sink available for air flow.

4.2 Variation of Thermal Resistance with Length of Fin and number of Fins

Figure 4 shows the 3-D and 2-D plot of thermal resistance with length of fins and number of fins. Clearly, there is a progressive decrease in thermal resistance with an increase in length of fin and an increase in number of fins. At a large length of fin, there is an increase in hydraulic diameter of the channel which will leads to a decrease in convective heat transfer coefficient. However there is a corresponding increase in heat transfer surface area which leads to reduction in the heat sink thermal resistance.

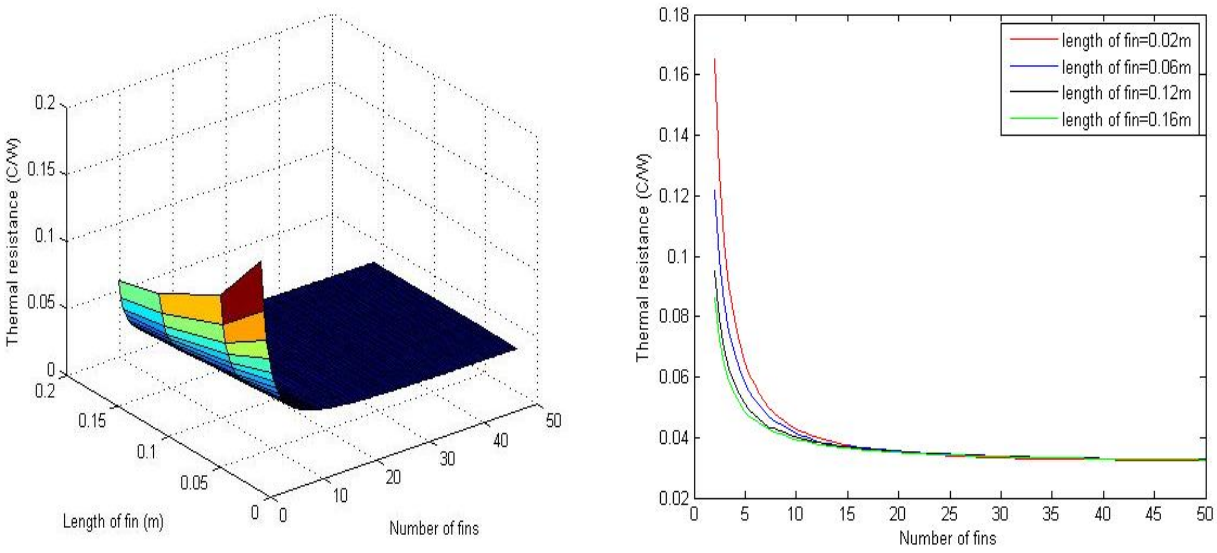

Fig. 4 Thermal Resistance Curves at various Length of Fin and number of Fins

Also at large numbers of fins, changes in length of fins have little influence on the thermal resistance of the heat sink. It must be pointed out that as the length of fin increases, and at large number of fins, there is a reduced heat exchange at the fin top, due to the temperature of the fin top approaching the ambient temperature.

4.3 Variation of Thermal Resistance with Length of Heat Sink and number of Fins

Figure 5 shows the 3-D and 2-D plot of thermal resistance with length of heat sink and number of fins. Clearly, low thermal resistance is achieved with a corresponding increase in length of heat sink and number of fins.

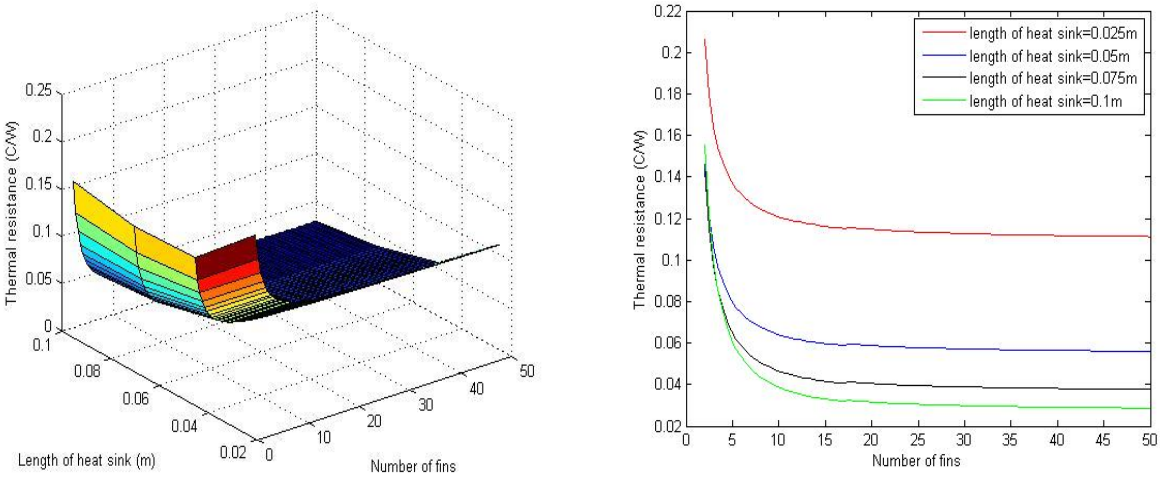

Fig. 5 Thermal Resistance Curves at various Length of heat sink and number of fins

The decrease in thermal resistance is due to the increase in the total fin surface area, and a corresponding increase in the average convective heat transfer coefficient. However, there would be an increase in pressure drop in the channel, which in turn leads to an increase in pumping power.

4.4 Variation of Thermal Resistance with Fin Thickness and number of Fins

Figure 6 shows the 3-D and 2-D plot of thermal resistance with fin thickness and number of fins. There is a gradual decrease in thermal resistance with an increase in fin thickness at constant number of fin.

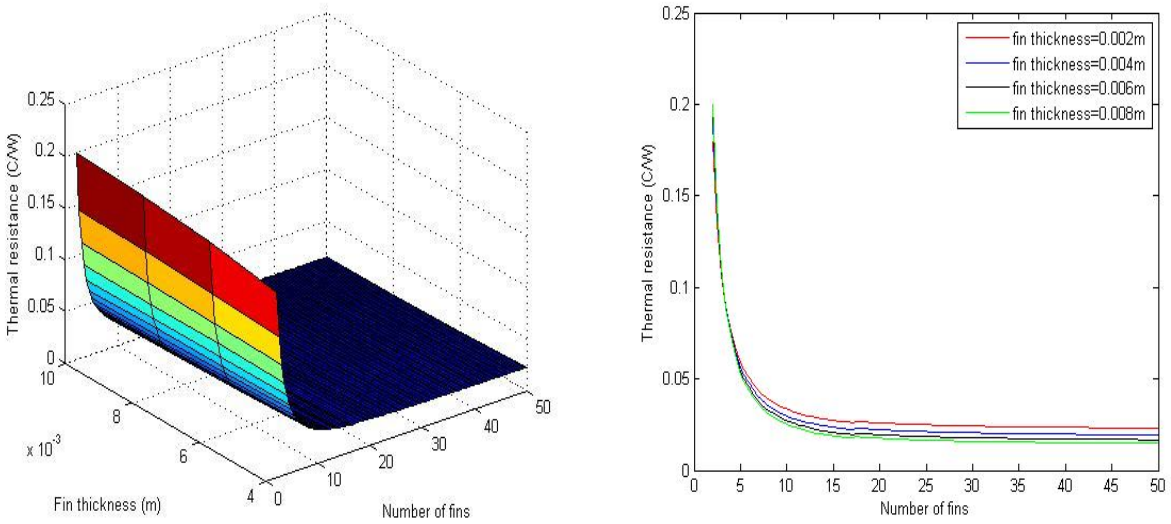

Fig. 6 Thermal Resistance Curves at various Fin Thickness and number of Fins

An increase in fin thickness allows heat flow through the whole length of the fin. A small fin thickness will not allow equal distribution of heat over the fin surface. This reduces the effective fin surface area, makes a part of the fin useless, and has associated manufacturing constraints. For a constant heat sink width, a compromise has to be made, as an increase in fin spacing will lead to corresponding decrease in fin thickness.

4.5 Variation of Thermal Resistance with Cross Sectional area and number of Fins

Figure 7 shows the 3-D and 2-D plot of thermal resistance with cross sectional area and number of fins. There is a gradual decrease in thermal resistance with an increase in cross sectional area at constant number of fin.

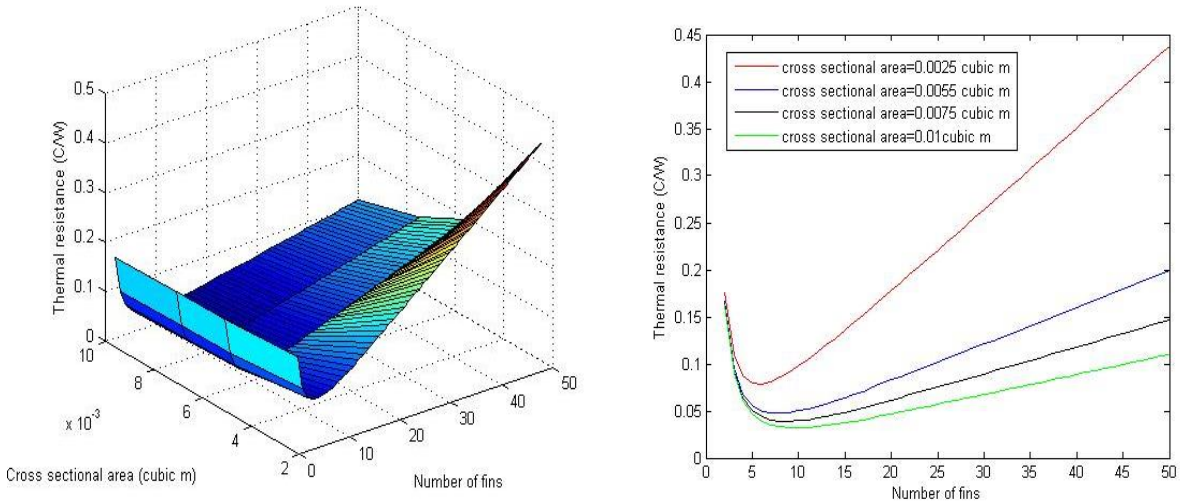

Fig. 7 Thermal Resistance with Cross Sectional Area and number of Fins

However, for each cross sectional area, there is an optimum number of fins beyond which the thermal resistance increases. Thus, small number of fins is desired as the cross sectional area increases.

The presented analysis shows that the performance of the heat sink can be maximized by selecting the correct profile. Due to the large number of variables, and the desire to minimize cost, weight and volume of heat sink, the least material approach was adopted.

In the optimization, the non dimensional parameters that are function of the independent variables are passed as global variables to the objective function. The resulting optimized heat sink variables are; fin spacing equal to 0.005m, fin length equal to 0.02m, number of fins equal to 10, fin thickness equal to 0.003m, heat sink length equal to 0.1m, heat sink base thickness equal to 0.004m, from which width of the heat sink equal to 0.075m, fin spacing ratio of 0.6667. The thermal resistance, fval, is equal to 0.0345 ^{o}C/W which is less than the thermal resistance of sink to ambient of the MOSFET Switch of 0.5063 ^{o}C/W, which clearly satisfy the heat sink model. The thermal management of the power inverter package yields experimental and modeled package temperatures of 34.7^{o}C and 36.5^{o}C respectively at air flow rate of 0.03065m^3/s.

5. Conclusion

Power inverters are essentially for supplying energy for today's society in a more efficient, sustainable and controllable manner. Thermally induced failures modes are the main causes of power inverter reliability issues. Thus the principal parameters that influence the performance of the heat sink are optimized for effective dissipation of the power losses in the inverter. In optimization of the heat sink, thermal performance is maximized and the weight satisfying constraint is minimized. Result of an actual test at 1500W corresponding to 75% of the inverter rating yields an experimental and modeled package temperatures of 34.7^{o}C and 36.5^{o}C respectively, recorded with the aid of MTM–380SD 3 Channels Temperature Monitor with SD Card Data logger, which shows that the optimized heat sink model works well and the inverter can safely and reliably be operated.

Nomenclature----------

A : Cross sectional area of heat sink, m^2
A_b : Base area of heat sink, m^2
A_{fa} : Convective surface area of air channel, m
B : Distance between first and last fins
C_p : Specific heat capacity, J/kgK
D : Heat sink base thickness, m
D_h : Hydraulic diameter, m
h_c : Convective heat transfer coefficient,W/m^{2}K
k : Thermal conductivity, W/mK
k_{al} : Thermal conductivity of heat sink material, W/mK
L : Heat sink length, m
L_f : Length of fin, m
n : Number of fins
Nu : Nusselt number
$\dot{V}$: Volume flow rate, m^3/s
v :Kinematic viscosity, m^2/s
P : Wetted perimeter, m
P_{dmax} : Maximum dissipated power,W
Pr : Prandtl's number
$\dot{Q}$: Convective heat transfer, W
Re : Reynold's number

$R_{t,hs}$: Thermal resistance of heat sink, $^oC/W$
$R_{t,sa}$: Thermal resistance of sink to ambient, $^oC/W$
$R_{t,jc}$:Thermal resistance of junction to case, $^oC/W$
$R_{t,cs}$: Thermal resistance of case to heat sink, $^oC/W$
S : Fin spacing, m
T_b : Base temperature, ^oC
T_c :Case temperature, ^oC
T_∞ :Ambient temperature, ^oC
T_f : Film temperature, ^oC
T_j : Junction temperature, ^oC
U : Velocity, m/s
μ : Dynamic viscosity, kg/ms
δ : Fin thickness, m
ρ : Density, kg/m^3

References

[1] Singh R., Baliga B. (1998). *Cryogenic Operation of Silicon Power Devices*. Kluwer Academic Publishers.
[2] Hannemann R., Fox L.R., Mahalingham M., (1991). Thermal Design for Microelectronic Components in Cooling Techniques for Components. *W. Aung, Hemisphere*, New York, pp. 245-276.
[3] Whitaker J. C. (1996). *The Electronics Hand Book* CRC Press pp. 441, 455, 484-486, 973-975.
[4] Ellison G.N., (1987). Thermal Computations for Electronic Equipment. *Van Nostrand Reinhold*, New York.
[5] Pang Y. E., Scott E. P., Chen J. E., Thole K. A. (2005). Thermal Design and Optimization Methodoly for Integrated Power Electronics Modules. *Journal of Electronic Packaging*, ASME, vol. 127, pp. 59-66.
[6] Mandel S. K., Sen D. (2016). A brief review on mixed convection heat transfer in channel flow with vortex generator for electronic chip cooling. *International Journal of Engineering Research and Application*, vol. 6, issue 6, pp. 74-82
[7] Ericsson (2000). Thermal Aspects on DC/DC Power Modules Design note: *Ericsson Microelectronics AB*, no. 004 pp. 1-8.
[8] Lostetter A., Barlow F., Elshabini A., (2000). An overview to Integrated Power Module design for high Power Electronics Packaging. *Microelectronics Reliability*, Vol.40, pp. 365-379.
[9] Xiao C., Ngo K., Lu G.-Q., (2009). Thermal Design of power Module to minimize peak Transient Temperature. In: *International Conference on Electronic Packaging Technology and High Density Packaging* (ICEPT-HDP), Xi'an, China pp. 248-254.
[10] Mokheimer E. M. A. (2003). Heat transfer from extended surfaces subject to variable heat transfer coefficient. *Heat and mass transfer* vol. 39, pp. 131-138.
[11] Shrirao P. N., Sherekar R. M., Bhalerao S. V. (2014). Evaluation of surface heat transfer coefficient for electronic packages. *International Journal of Research in Advent Technology*, vol. 2. Issue 1, pp. 59-66.
[12] Furkay S.S. (1984). Convective heat transfer in Electronic Equipment: An overview, In Thermal
[13] Management Concepts in Microelectronic Packaging. *ISHM Technical Monograph* Series 6984-003,
[14] Silver spring, MD., pp. 153-179.
[15] Kern D.Q., Kraus A.D. (1972). *Extended Surface Heat transfer.* McGraw-Hill, New York.
[16] Baehr H. D., Stephen K., (1998). *Heat and Mass Transfer.* ISBN 3-540-64458-X, 3rd Edition, Springer, pp. 220-221,259-262, 350-355.
[17] Buller M.L., Kilburn R.F., (1981). Evaluation of surface heat transfer coefficients for Electronic modular packages in Heat Transfer in Electronic Equipment. *HTD*, Vol. 20, pp. 25-28, ASME, New York.
[18] Tritt T.M. (2004). *Physics of Solids and Liquids Thermal Conductivity: Theory, properties and Applications.* Second Edition, New York, NY: Kluwer academic/plenum publishers Vol. 1.
[19] Rogers G.F.C., and Mayhew Y.R., (1966). *Engineering Thermodynamics Work and Heat Transfer.* 4th edition, Longman pp. 509-518.
[20] Eastop T.D., Mckonkey A. (1999). *Applied Thermodynamics for Engineering Technologies*. 5th edition, Pearson Education, pp. 577-583.